Journal of Colloid and Interface Science 511 (2018) 243–250

Contents lists available at ScienceDirect

Journal of Colloid and Interface Science

journal homepage: www.elsevier.com/locate/jcis

Regular Article

Green synthesis of highly dispersed ytterbium and thulium co-doped sodium yttrium fluoride microphosphors for *in situ* light upconversion from near-infrared to blue in animals

Yuan Pu [a,b], Lifeng Lin [a], Dan Wang [a,b,*], Jie-Xin Wang [a,c], Jun Qian [d], Jian-Feng Chen [a,b,c]

[a] State Key Laboratory of Organic-Inorganic Composites, Beijing University of Chemical Technology, Beijing 100029, China
[b] Research Centre of the Ministry of Education for High Gravity Engineering and Technology, Beijing University of Chemical Technology, Beijing 100029, China
[c] Beijing Advanced Innovation Center for Soft Matter Science and Engineering, Beijing University of Chemical Technology, Beijing 100029, China
[d] State Key Laboratory of Modern Optical Instrumentation, Centre for Optical and Electromagnetic Research, Zhejiang Provincial Key Laboratory for Sensing Technologies, Zhejiang University, 310058 Hangzhou, China

GRAPHICAL ABSTRACT

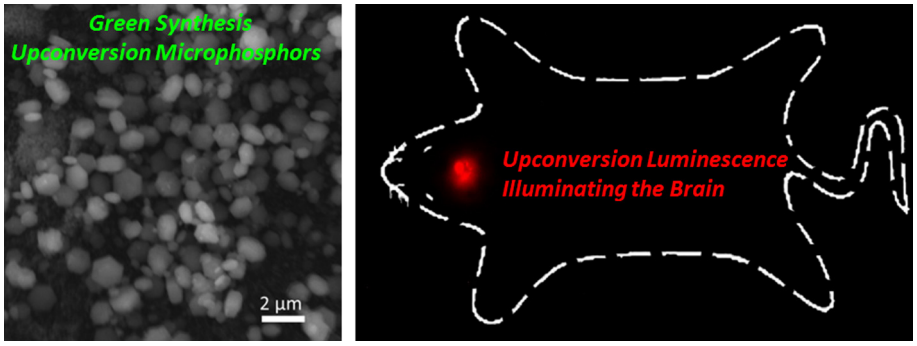

ARTICLE INFO

Article history:
Received 8 August 2017
Revised 5 October 2017
Accepted 5 October 2017
Available online 7 October 2017

Keywords:
Green synthesis
$NaYF_4$:Yb^{3+}, Tm^{3+} microphosphors
Near-infrared
Upconversion luminescence
In vivo
Brain imaging

ABSTRACT

We report a simple, low cost and environmentally friendly method to prepare $NaYF_4$:Yb^{3+}, Tm^{3+} upconversion microphosphors (UCMPs) by thermal decomposition of rare earth-trifluoroacetate precursors using paraffin as the high boiling non-coordinating solvent. The UCMPs exhibited cubic phase with defined shape and bright upconversion luminescence. After coating with amphiphilic polymers of phospholipid-polyethylene glycol, the $NaYF_4$:Yb^{3+}, Tm^{3+} UCMPs were highly dispersed in aqueous solutions and exhibited low cytotoxicity. Furthermore, we explored the use of the micro-injected micro-sized $NaYF_4$:Yb^{3+}, Tm^{3+} particles for converting of near infrared into blue light in mice brain. The *in vivo* macroscopic upconversion luminescence imaging results showed that UCMPs located at 1 mm depth in the brain could be clearly distinguished. Microscopic upconversion luminescence imaging of the brain sections *in vitro* revealed that the UCMPs embedded at the particular location in brain tissues of mice were stable without significant diffusion in two weeks.

1. Introduction

Rare-earth doped upconversion phosphors, which convert low energy near-infrared (NIR) light into high-energy ultraviolet or vis-

* Corresponding author at: State Key Laboratory of Organic-Inorganic Composites, Beijing University of Chemical Technology, Beijing 100029, China.
E-mail address: wangdan@mail.buct.edu.cn (D. Wang).

https://doi.org/10.1016/j.jcis.2017.10.017
0021-9797/

ible light, have recently attracted increasing attention in bio-related applications [1–3]. In comparison with traditional luminescent materials, such as organic dyes [4,5] and quantum dots (QDs) [6–8], the emission of upconversion phosphors were generated by excitation of continuous wave NIR laser, which was beneficial for enhancement the penetration depth and minimizing the autofluorescence of biological tissues [9–11]. Therefore, rare-earth doped upconversion nanophosphors (UCNPs) have been widely utilized to light-up the cells in deep tissues for fluorescence diagnosis [12–14], photodynamic therapy [15], and optogenetics [16]. However, the low upconversion efficiency of UCNPs is still far from perfect for such applications, particularly for optogenetics manipulations, which have an excitation light threshold for activation [17]. For photoactivation applications such as fluorescence diagnosis and photodynamic therapy, the phosphors are usually given by intravenous injection and should be small enough for long-time circulation in animals. In comparison, for optogenetics applications, the phosphors are expected to be embedded at a particular location in the neuronal plasma membrane, where the neurons are controlled by the exogenous expression of light-sensitive ion channels. Hence, when using upconversion phosphors for optogenetic applications, the phospors should be designed with high upconversion efficiency for photoactivation and suitable sizes to avoid their diffusion in tissues. Comparing with rare earth doped UCNPs, upconversion microphosphors (UCMPs), which are much larger in size, usually present stronger upconversion emission due to their smaller surface-to-volume ratio and less surface quenching centers [18], promising for applications in optogenetic studies. Although powders of UCMPs are commercially available and used in for the visualization of IR radiation and security inks, they cannot be well suspended in aqueous or organic solutions to form colloidal dispersions, which limit their extending applications [19]. Thus, it is still valuable to explore facile methods for synthesis of highly dispersed UCMPs [20].

Upconversion phosphors are typically composed of an inorganic host lattice and rare-earth dopant ions embedded in the host lattice. Sodium yttrium fluoride ($NaYF_4$) has been widely used as a host in upconversion luminescence process due to its appropriate lattice matching with sensitizing ion (Yb^{3+}) and activating ions (Er^{3+}, Tm^{3+}, Ho^{3+}) high efficient upconversion phosphors [21]. Thus far, many approaches have been developed to synthesis rare-earth doped $NaYF_4$ upconversion phosphors with high quality, low cost and minimal toxicity [22–24]. The majority of these methods are substantially based on the thermal decomposition of rare earth-trifluoroacetate precursors in high boiling noncoordinating solvents (e.g., octadecene [25], trioctylphosphine [26]) or liquid precipitation reaction between soluble rare-earth salts and alkali fluorides. Along with others, we have reported the synthesis of lanthanide-doped rare-earth fluorides UCNPs by using eco-friendly paraffin liquid, instead of 1-octadecene, as the high boiling noncoordinating solvent [27,28]. However, as far as we are aware, the synthesis of $NaYF_4$:Yb^{3+}, Tm^{3+} microphosphors has been rarely reported.

In this paper, we report a green route for the synthesis of highly dispersed $NaYF_4$:Yb^{3+}, Tm^{3+} UCMPs by thermal decomposition of rare earth-trifluoroacetate precursors at 320 °C under ambient air pressure without inert gas protection. The paraffin liquid was employed as the high boiling noncoordinating solvent for the reactions and citric acid was used as the surface active agent. Both paraffin liquid and citric acid are natural products, with no toxicity and no environmental pollution [29], which are beneficial for wide-scale preparation of UCMPs. The UCMPs were then coated with amphiphilic polymers to form hydrophilic hybrid composites, abbreviated UCMPs@PEG. The morphology, structure and upconversion luminescence property of the UCMPs and UCMPs@PEG were investigated by scanning electronic microscope (SEM), transmission electron microscope (TEM), powder X-ray diffraction (XRD), Fourier transform infrared (FTIR) spectrophotometry, thermogravimetric analysis (TGA) and luminescence spectra measurements. The cytotoxicity of UCMPs@PEG was determined by *in vitro* cell studies. Furthermore, the UCMPs@PEG particles were microinjected into the brain of mice. Macroscopic upconversion luminescence imaging of mice *in vivo* were carried out to investigate the abilities of the UCMPs@PEG for *in situ* light upconversion from near-infrared to blue in mice. Microscopic upconversion luminescence imaging of the brain sections *in vitro* were performed to study the long-term distribution of UCMPs@PEG in brain tissues of mice.

2. Experimental

2.1. Materials and instruments

Lanthanide oxides (Y_2O_3, Yb_2O_3, Tm_2O_3), trifluoroacetic acid, sodium fluoride, oleic acid, paraffin, chloroform, ethanol, and methanol were purchased from the Sigma Aldrich. 1,2-distearoyl-*sn-glycero*-3-phosphoethanolamine-N-[methoxy(polyethylene glycol)-5000] (PEG) was purchased from Creative PEGWorks, Inc. Cell-culture products were purchased from Gibco. All the chemicals were used without any additional purification unless otherwise mentioned. Deionized water prepared by a Hitech Laboratory Water Purification System DW100 (Shanghai Hitech Instruments Co., Ltd) was used for all experiments.

The morphology studies were performed using a JEOL JSM-6360LV scanning electron microscope (SEM) and a Hitachi HT-7700 transmission electron microscope (TEM). The average size of the particles was calculated by measuring 100 particles from SEM and TEM images. X-ray powder diffraction (XRD) was carried out on a Japan Rigaku D/max rA X-ray diffractometer equipped with a Cu Kα radiation. Dynamic light scattering (DLS) and zeta potential measurements were conducted by using a Malvern Zetasizer Nano ZS90 instrument. Triplicate samples were measured three times each at room temperature. The measurements were initiated within 3 min after sample preparation. Fourier transform infrared (FTIR) spectra were collected using a PerkinElmer spectrum GX FTIR system. A TA Instrument with a heating rate of 10 °C was used for the thermogravimetric analysis (TGA). Luminescence spectra of the $NaYF_4$ microphosphors was measured with a PG2000 spectrometer (Ideaoptics Instruments, China), using a 980 nm laser as the excitation light. *In vivo* luminescence imaging of mice was performed on a Maestro *in vivo* optical imaging system (CRI, Inc. Woburn, MA) equipped with a commercial 980 nm laser. Luminescence imaging of the brain slices of mice were acquired using an Olympus FV1000 laser confocal microscope equipped with a 980 nm laser.

2.2. Synthesis of $NaYF_4$:Yb^{3+}, Tm^{3+} upconversion microphosphors

In a typical synthesis approach of $NaYF_4$:Yb^{3+}, Tm^{3+} UCMPs, 0.025 mmol Tm_2O_3, 0.25 mmol Yb_2O_3, and 0.975 mmol Y_2O_3 were added to 20 mL of 50 % concentrated trifluoroacetic acid in a 250 mL flask. The mixture solution was heated to 80 °C to form a homogeneous solution and then slowly evaporated to remove water and excess trifluoroacetic acid, forming muddy mixture of $RE(CF_3COO)_3$ (RE = Y, Yb, and Tm). Subsequently, 4.5 mmol NaF, 10 mL oleic acid and 30 mL paraffin liquid were added to the flask under vigorous stirring conditions and the mixture solution was slowly heated to 140 °C under vacuum for 20 min to remove water. The resulting solution with a slight yellow color was then heated to 320 °C at a rate of 10 °C/min in air and was kept at 320 °C for 1 h. Finally, the mixture was cooled to room temperature and precipi-

tated by methanol and collected by centrifugation at 12000 rpm for 30 min. The precipitate was washed with ethanol for three times and the obtained microphosphors of $NaYF_4$:Yb^{3+}, Tm^{3+} were dried in a vacuum oven for 24 h.

2.3. Preparation of DSPE-mPEG coated $NaYF_4$:Yb^{3+}, Tm^{3+} upconversion microphosphors

Typically, 400 μL dispersion of $NaYF_4$:Yb^{3+}, Tm^{3+} UCMPs in chloroform (10 mg/mL) was injected into 1 mL DSPE-mPEG solution in chloroform (10 mg/mL). The mixture solution was then evaporated and dried under vacuum in a rotary evaporator, following which the residuum was gently heated at 70 °C. Next, 500 μL of water was added to the obtained solid mass, and the solution was sonicated for 1 min. The resulting DSPE-mPEG coated $NaYF_4$:Yb^{3+}, Tm^{3+} UCMPs (UCMPs@PEG) were stored at 4 °C for further use.

2.4. Cytotoxicity analyses

The mouse fibroblast cell lines (NIH-3T3) were used for cytotoxicity studies of DSPE-mPEG coated upconversion microphosphors. The cells were grown in Dulbecco minimum essential medium (DMEM) supplemented with 10% heat-inactivated fetal bovine serum and seeded in 35 mm cultivation dishes. The cells were divided at random into 5 groups, and each group contained 6 dishes of cells. Pre-determined amounts of UCMPs@PEG were added to the five groups of cells to achieve a final concentration of 0, 50, 100, 150 and 200 μg/mL, respectively. After the cells were incubated with UCMPs@PEG for 24 h and 48 h, the viabilities of the cells were assessed by 3-(4,5-Dimethyl-2-thiazolyl)-2,5-diphenyl-2H-tetrazolium bromide (MTT) assay [30]. We assumed that the viability of control cells without UCMPs@PEG treatment was 100%, and estimated the relative viability of cells treated with UCMPs@PEG of various concentrations. The data shown is an average of three experiments.

2.5. In vivo imaging

Five experimental mice (18–21 g male black mice, C57 line) were microinjected with 0.2 μL aqueous dispersion of UCMPs@PEG (0.2 μL per mouse, 1 mg/mL in 1 × PBS, pH = 7.4) through microsurgery. The relatively accurate XY-Z (depth) position where the UCMPs@PEG particles located was determined by counting the scale on the microinjection instrument [31]. In our experiment, the depth of injected UCMPs@PEG particles was adjusted as 1 mm. The *in vivo* upconversion luminescence imaging of UCMPs@PEG in the brain of mice was carried out by Maestro *in vivo* optical imaging system (CRI, Inc. Woburn, MA), equipped with a 980 nm laser (LWIR980nm, Beijing Laserwave Optoelectronics Technology Co., Ltd, China). A liquid crystal tunable filter was automatically tuned with 10 nm increments from 700 nm to 900 nm while the camera captured the image at each wavelength with a constant exposure time (500 ms).

3. Results and discussion

The synthesis of $NaYF_4$:Yb^{3+}, Tm^{3+} nanophosphors by thermal decomposition route has been intensively investigated in the past decade, but seldom have the chemical reaction equations been put forward in the literature. In Fig. 1a, we present the possible process and chemical reactions involved in the formation of $NaYF_4$:Yb^{3+}, Tm^{3+} crystals in our route. Generally, rare earth-trifluoroacetate precursors ($RE(CF_3CO_2)_3$) were prepared using lanthanide oxides (RE_2O_3) and trifluoroacetic acid (CF_3CO_2H) by double decomposition reaction. The thermal decomposition of $RE(CF_3CO_2)_3$ in paraffin liquid at 320 °C produced REF_3 seeds and gases (i.e. CF_3COF, CO and CO_2). At the same time, the REF_3 reacted with Na+ and F− to generate $NaREF_4$ crystal nuclei, which then quickly grew via the Ostwald ripening process, resulting $NaREF_4$ microcrystals with well-defined cross sections. The carboxy groups of oleic acid could coordinate with electronpoor metal atoms at the surfaces of the $NaREF_4$ crystals while the exposed hydrophobic alkyl chain on the surface enabled the $NaREF_4$ microparticles to be dispersed in nonpolar solvents. The paraffin was adopted as the solvent, which made environment pollution reduced and production cost decreased, compared with the previous route for $NaYF_4$ using octadecene as the solvent.

Fig. 2a–c shows the morphology of UCMPs investigated by both SEM and TEM, which demonstrated that the as-synthesized UCMPs were hexagonal prism shaped particles with average side length of 1 ± 0.18 μm and thickness of 0.5 ± 0.1 μm (Fig. 2d). The XRD pattern of as-synthesized UCMPs was shown in Fig. 2e. All the peak positions agree well with those calculated for the cubic phase of $NaYF_4$ crystal (JCPDS 39-0724). The well-resolved four peaks between 20° and 60° in 2θ value could be assigned to (1 1 1), (2 0 0), (2 2 0), and (3 1 1) planes of cubic $NaYF_4$ crystal. Fig. 2f shows the TGA curve of UCMPs in air. The significant weight loss of UCMPs in the temperature range of 300–500 °C was attributed to the elimination of oleic acid ligands. X-ray energy dispersive spectroscopy (EDS) spectrum taken from the UCMPs (Fig. S1) confirm that the particles mainly consisted of Na, F, Y and Yb. The C and O elements were also detected, which were attributed to the oleic acid molecules on the surface of the UCMPs. However, the Tm elements were not detected due to the limited sensitivity of the EDS measurements. The proportion of the elements for UCMPs (Table S1) was different than the feed reactants, which was caused by the low efficiency of mass transfer in the flask. Development of novel reactors with high mass transfer efficiency for preparation of UCMPs should be an interesting topic for follow-up studies [11].

Fig. 3a shows the schematic illustration for the preparation of UCMPs@PEG composites. During the mixing of solid lipidic mass (i.e. UCMPs and DSPE-mPEG-5000) and addition of water under continuous sonication, the hydrophobic lipid segments of DSPE-mPEG-5000 tended to be embedded in the hydrophobic UCMPs core and the hydrophilic PEG chains of DSPE-mPEG-5000 extended into the aqueous phase to render the UCMPs@PEG with water dispersibility and excellent biocompatibility [32]. Fig. 3b presents a typical SEM image of UCMPs@PEG particles, from which we could see the UCMPs@PEG exhibited similar morphology with UCMPs and particles were highly dispersed with no significant aggregates observed. The inset of Fig. 3b shows a typical digital photo of water-based suspension containing UCMPs@PEG (1 mg/mL), which was milky white translucent solution, due to the light scattering by microparticles. The monodispersity of UCMPs@PEG in an aqueous environment was also confirmed by DLS measurements. Two peaks of the size distribution (intensity) were observed due to the prism shape of UCMPs@PEG (Fig. 3c). The two peaks were located at around 580 nm and 900 nm respectively, which were essentially in agreement with the average thickness and average side length of UCMPs observed by SEM. The average zeta potential of UCMPs@PEG in aqueous solution was measured to be −20.7 ± 5.9 mV (Fig. S2). The negative charge was attributed to the PEG coating on the surface of UCMPs and can repel one another to overcome the natural tendency of aggregation of particles [33,34]. Therefore, PEG coated UCMPs@PEG present engouth dispersion stability in aqueous solution. It was also reported that NPs with negatively charged surface showed a reduced plasma protein adsorption and low rate of nonspecific cellular uptake [35,36]. Although it is difficult to observe the thin layer of PEG on the surface of UCMPs in either SEM or TEM images due to the low electron contrast between the PEG layer and UCMPs, the presence of a PEG layer

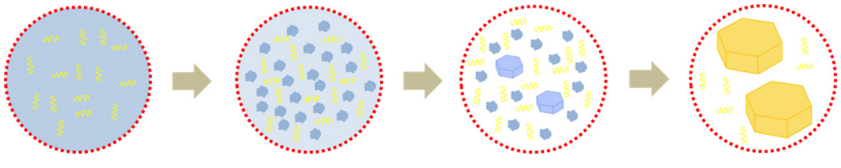

$$RE_2O_3+6CF_3CO_2H \xrightarrow{\triangle} 2RE(CF_3CO_2)_3+3H_2O$$

$$2RE(CF_3CO_2)_3 \xrightarrow{\triangle} 2REF_3+3CF_3COF\uparrow+3CO\uparrow+3CO_2\uparrow$$

$$REF_3 + Na^+ + F^- \longrightarrow NaREF_4$$

RE= Y, Yb, Tm…

Fig. 1. Schematic diagram of the process and possible chemical reactions involved in the formation of $NaYF_4$:Yb^{3+}, Tm^{3+} UCMPs.

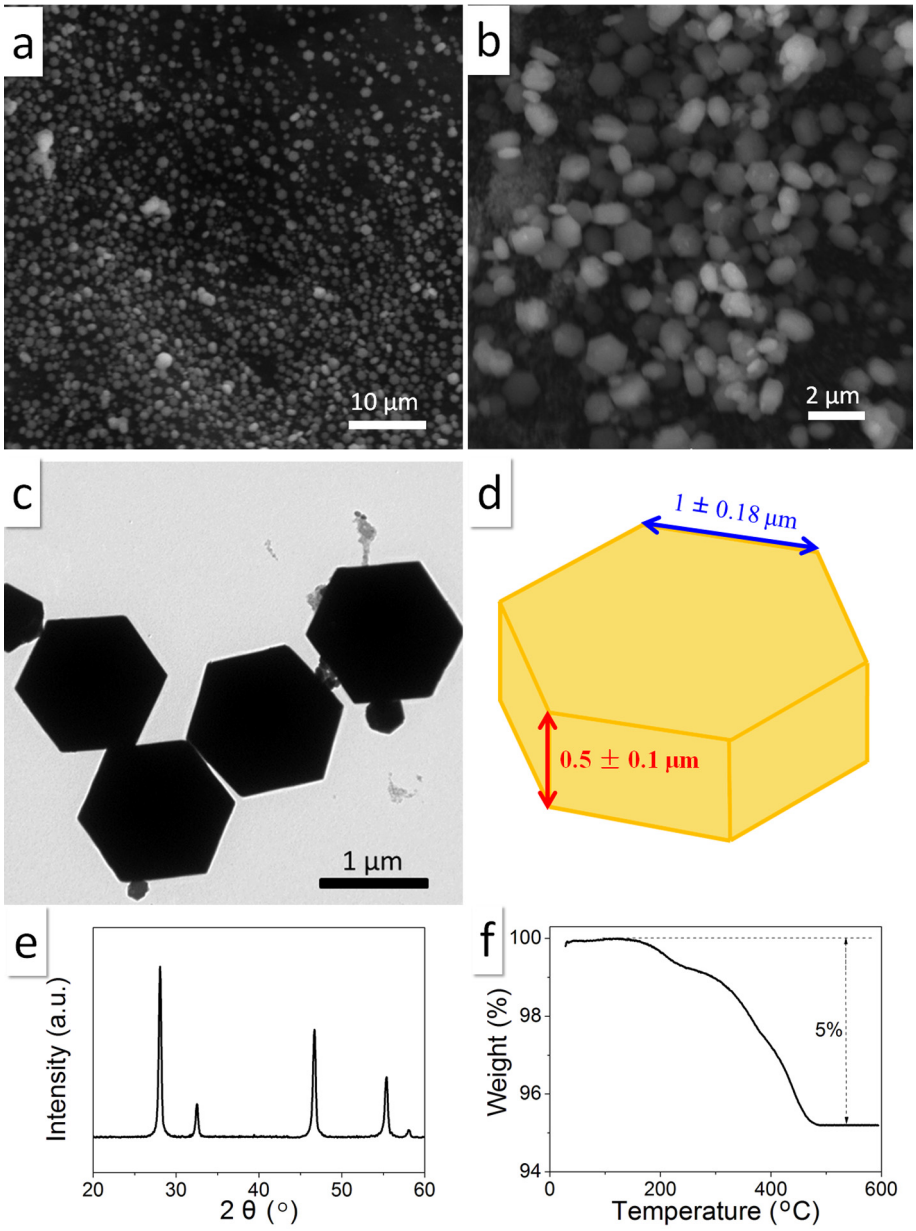

Fig. 2. SEM (a, b) and TEM (c) images of as-synthesized UCMPs; (d) shape and size illustration of the UCMPs; XRD pattern (e) and TGA curve (f) of the UCMPs.

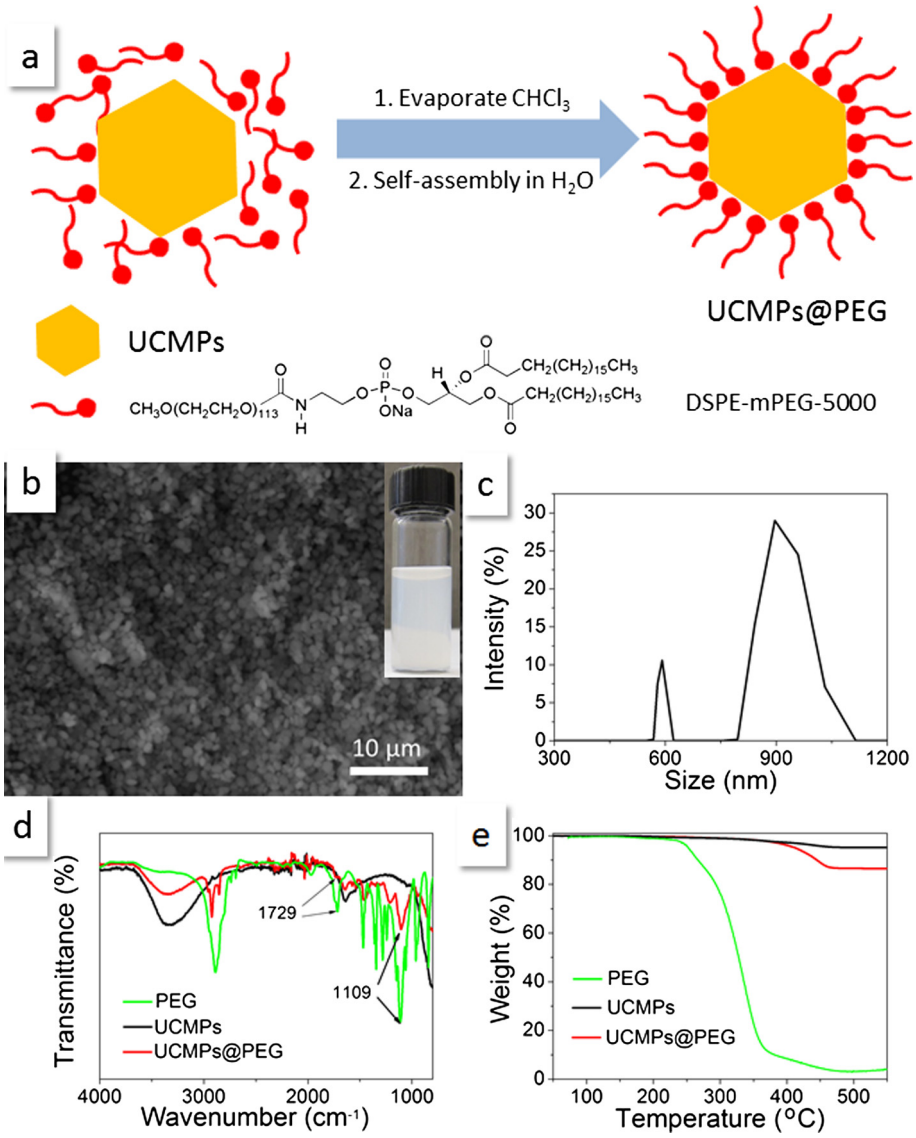

Fig. 3. (a) Schematic illustration of UCMPs@PEG preparation from self-assembly; (b) a typical SEM image of the obtained UCMPs@PEG particles; the inset: a digital photo of UCMPs@PEG dispersion in water (1 mg/mL); (c) DLS results of UCMPs@PEG in water (1 mg/mL); (d) FTIR spectra and (e) TGA curves of PEG, UCMPs and UCMPs@PEG.

on the UCMPs was confirmed by FTIR and TGA. Fig. 3d shows the spectra of PEG, UCMPs and UCMPs@PEG. Both of the UCMPs and UCMPs@PEG demonstrated a broad absorption band over 3000 cm^{-1}, which corresponds to the O-H stretching vibration. The peaks at around 2920 cm^{-1} were significantly increased in the UCMPs@PEG sample due to a large number of -CH_2- groups in the PEG coating. In addition, two bands at 1729 and 1109 cm^{-1} in the FTIR spectrum of UCMPs@PEG were observed, which were assigned to the stretching vibration of the carboxyl ester and the ether bond of PEG chains, respectively [37,38]. These results demonstrated the successfully coating of PEG on the surface of UCMPs. From the TGA curve of UCMPs@PEG in Fig. 3e, the weight loss of the UCMPs@PEG in the temperature range of 300–500 °C was much larger than that of UCMPs, due to the PEG coating on UCMPs. The UCMPs/PEG weight ratio in the UCMPs@PEG was determined to be about 9:1 according to the TGA results. The XRD pattern of UCMPs@PEG in Fig. S3 exhibited the same structure as UCMPs in Fig. 2e, demonstrating that the crystal structure of UCMPs was not affected by the PEG coating.

Fig. 4a shows a typical upconversion luminescence spectrum of $NaYF_4$:Yb^{3+}, Tm^{3+} microphosphors under the excitation of a 980 nm laser. The sample exhibits five upconversion emission peaks including a strong NIR emission peak at 800 nm, two blue emission peaks at 450 nm and 475 nm, and two weak red emission peaks at 650 nm and 700 nm. The insert of Fig. 4a shows a digital photo of UCMPs@PEG aqueous suspension under a 980 nm laser excitation, exhibiting bright blue luminescence, which was in agreement with the upconversion luminescence spectrum in the visible range. It is generally known that Tm^{3+} ions serve as the activator to generate tunable upconversion emissions spanning the visible spectral region [1,2]. Yb^{3+} ions are added to serve as a sensitizer that enhances the infrared-to-visible upconversion efficiency due to the strong energy transfer from Yb^{3+} to neighboring Tm^{3+} ions [3]. $NaYF_4$ is the host, which shows no upconversion emission under NIR light excitation. Fig. 4b shows the energy level diagrams of Yb^{3+} and Tm^{3+} ions and the upconversion luminescence mechanism of sample under the excitation of 980 nm. The upconversion emission peaks of $NaYF_4$:Yb^{3+}, Tm^{3+} at 450, 475, 650, 700, and 800 nm correspond to the $^1D_2 \rightarrow {}^3F_4$, $^1G_4 \rightarrow {}^3H_6$, $^1G_4 \rightarrow {}^3F_4$, $^3F_3 \rightarrow {}^3H_6$ and $^3F_4 \rightarrow {}^3H_6$. transitions of Tm^{3+} ions, respectively [34].

To investigate potential bio-related applications for the UCMPs@PEG, we performed *in vitro* cytotoxicity studies on the UCMPs@PEG in terms of cell viability by MTT assay. The

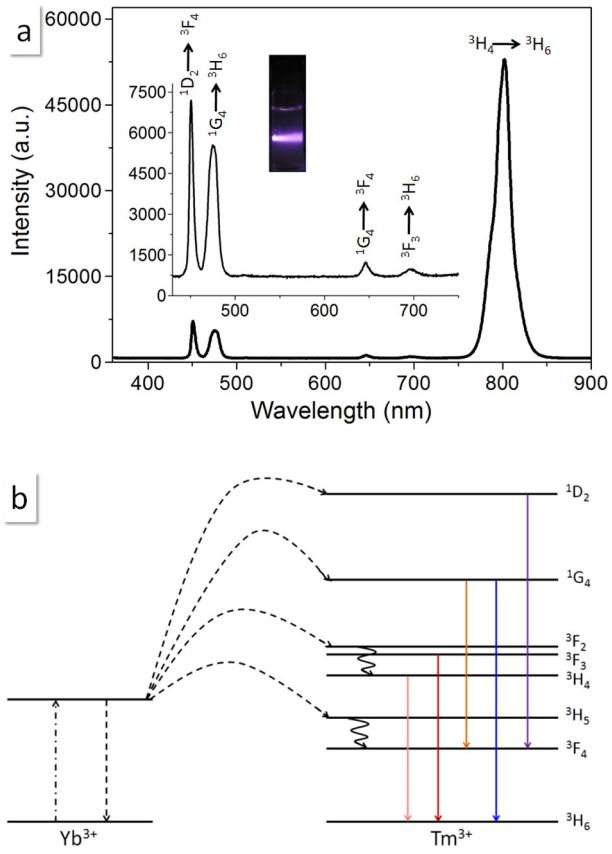

Fig. 4. (a) Typical upconversion luminescence spectrum of $NaYF_4$:Yb^{3+}, Tm^{3+} UCMPs@PEG excited by a 980 nm CW laser. Inset: a digital photo of aqueous dispersion of UCMPs@PEG under irradiation of 980 nm CW laser; (b) Energy level diagrams of Yb^{3+} and Tm^{3+} ions and the probable upconversion mechanism under the excitation of 980 nm light.

relative cell viabilities of NIH-3T3 cells treated with UCMPs@PEG at various concentrations after 24 h and 4 h incubation were shown in Fig. 5. Even when cells were incubated with UCMPs@PEG (200 μg/mL) for up to 48 h, no significant decrease in cell viability was observed, indicating a low cytotoxicity for the UCMPs@PEG.

Due to the unique upconversion luminescence by NIR excitation which was beneficial for enhancement the penetration depth,

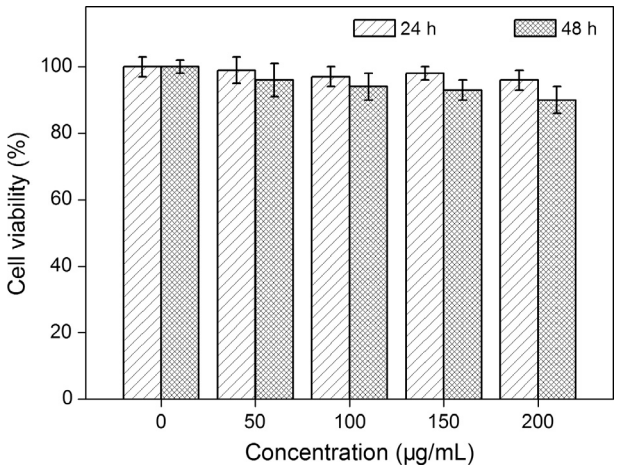

Fig. 5. Cell viability from MTT assays of NIH-3T3 cells incubated with UCMPs@PEG at various concentrations for 24 h and 48 h, respectively. Error bars represent the standard deviation of the mean.

$NaYF_4$:Yb^{3+}, Tm^{3+} phosphors, especially upconversion nanophosphors, have been utilized for various biomedical applications, such as fluorescence diagnosis, photodynamic therapy, and optogenetics. Although the UCMPs exhibited bright upconversion luminescence, they were too large to be given by intravenous injection in animals for targeted diagnosis. As for optogenetics, the phospors are expected to be embedded at a particular location and should be large enough to avoid their diffusion in tissues. In this work, we performed the *in vivo* upconversion luminescence imaging of mice after microinjection of UCMPs@PEG in the brain tissue of mice (Fig. 6a). The depth of the UCMPs@PEG in the brain was 1 mm in our experiments. Fig. 6b shows the whole body *in vivo* image of a black mouse injected with UCMPs@PEG, from which

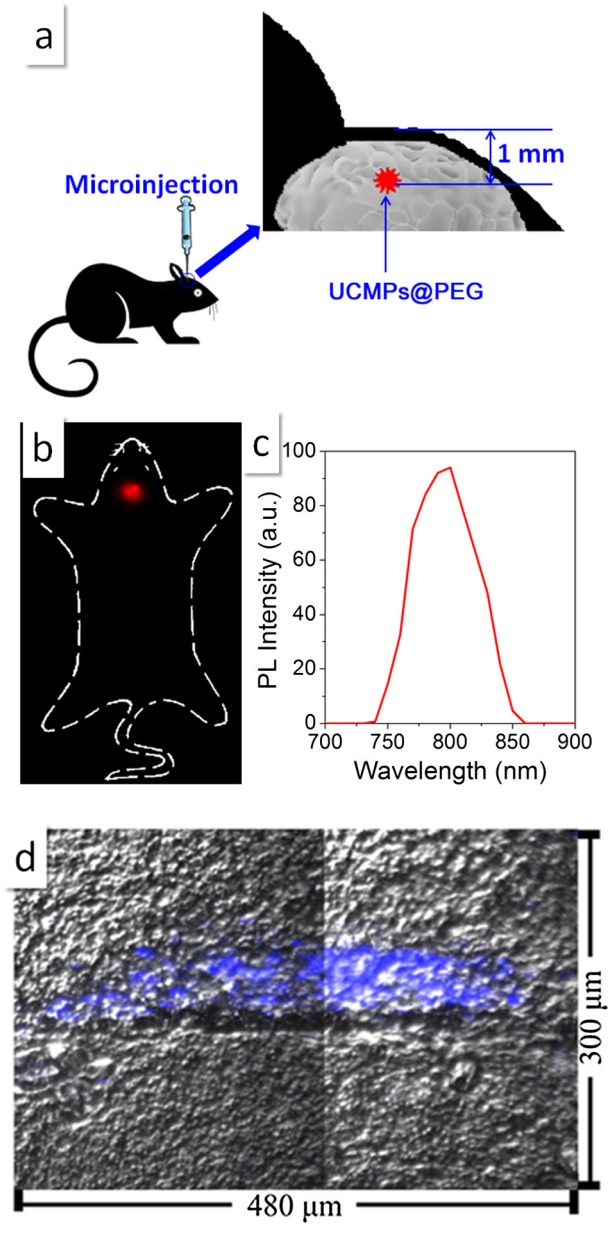

Fig. 6. (a) A diagram of microinjection of UCMPs@PEG particles in a mouse brain; (b) *in vivo* upconversion luminescence imaging of mice injected with UCMPs@PEG particles under excitation of 980 nm light; (c) spectra of the luminescence signal from UCMPs@PEG in mice brain observed in (b); (d) a typical upconversion luminescence image of the brain tissue slice from mice injected with UCMPs@PEG particles in the brain for 2 weeks. The blue color revealed the distribution of UCMPs@PEG particles.

the emission of UCMPs@PEG was observed with high contrast. It is generally known that the skin, tissues, blood and trauma region of mice present no autofluorescence in the visible light region when excited by 980 nm NIR laser [39]. Therefore, the observed luminescence signals were generated from the UCMPs@PEG particles. The upconversion luminescence spectrum of the UCMPs@PEG (Fig. 6c) with a wavelength range from 700–900 nm also testifies that the 980 nm laser light greatly excited the UCMPs@PEG to emit upconversion luminescence. In general, the distribution depth of cerebellum and cerebral cortex of small mice were less than 800 μm in their brains [31]. UCMPs can achieve such a depth for *in situ* light upconversion from near-infrared to blue, and it will be very helpful to potential *in vivo* optogenetic applications. To investigate the long-term distribution of UCMPs@PEG in brain tissues of mice, the mice was put down after microinjection of UCMPs@PEG for two weeks, and their brain sections were imaged by microscopic upconversion luminescence imaging. As a typical image shown in Fig. 6d, the UCMPs@PEG distribution was concentrated a very small area of 500 μm × 500 μm × 50 μm. These primary results demonstrated the potential of using $NaYF_4$:Yb^{3+}, Tm^{3+} microphosphors for *in vivo* optogenetic studies.

4. Conclusion

We developed a simple and green route for the synthesis of highly dispersed $NaYF_4$:Yb^{3+}, Tm^{3+} UCMPs. The paraffin, an eco-friendly solvent, was used as the high boiling non-coordinating solvent during the thermal decomposition of rare earth-trifluoroacetate precursors. Choosing paraffin as the reaction medium without expensive and not environmentally friendly octadecene, significantly simplified the reaction for green and low-cost synthesis of the $NaYF_4$:Yb^{3+}, Tm^{3+} UCMPs. Furthermore, we explored the use of the PEG coated $NaYF_4$:Yb^{3+}, Tm^{3+} UCMPs for converting of near infrared into blue light in mice brain, based on their bright upconversion luminescence and low cytotoxicity. The *in vivo* macroscopic upconversion luminescence imaging results showed that UCMPs located at 1 mm depth in the brain could be clearly distinguished. The long-term distribution of UCMPs@PEG in brain tissues of mice were investigated by microscopic upconversion luminescence imaging of the brain sections, demonstrating that the UCMPs@PEG were stable without significant diffusion in two weeks. Compared with upconversion nanoparticles that are easily uptaken by cells [40] or flow into circulatory systems [41], the UCMPs are large enough to be fixed at a specific locations without diffusion in tissues, facilitating the *in situ* light conversion at that particular area of the cortex in animals. Our demonstration represents a new strategy to utilize the upconversion phosphors for biomedical studies. Further investigations are underway to investigate the potential applications of rare-earth doped upconversion microstructures in optogenetic studies.

Acknowledgments

This work was supported by the National Key Research and Development Program of China (2016YFA0201701/2016YFA0201700), National Natural Science Foundation of China (21622601), the Fundamental Research Funds for the Central Universities (BUCTRC201601), and the "111" project of China (B14004).

Conflict of interest

The authors declare no competing financial interest.

Appendix A. Supplementary material

Supplementary data associated with this article can be found, in the online version, at https://doi.org/10.1016/j.jcis.2017.10.017.

References

[1] J. Zhou, Q. Liu, W. Feng, Y. Sun, F.Y. Li, Upconversion luminescent materials: advances and applications, Chem. Rev. 115 (2015) 395–465.
[2] L. Cheng, C. Wang, Z. Liu, Upconversion nanoparticles and their composite nanostructures for biomedical imaging and cancer therapy, Nanoscale 5 (2012) 23–37.
[3] H. Dong, S.D. Du, X.Y. Zheng, G.M. Lyu, L.D. Sun, L.D. Li, P.Z. Zhang, C. Zhang, C. H. Yan, Lanthanide nanoparticles: from design toward bioimaging and therapy, Chem. Rev. 115 (2015) 10725–10815.
[4] D. Wang, J. Qian, S. He, J.S. Park, K.S. Lee, S.H. Han, Y. Mu, Aggregation-enhanced fluorescence in PEGylated phospholipid nanomicelles for *in vivo* imaging, Biomaterials 32 (2011) 5880–5888.
[5] M.W. Wang, N. Yang, Z.Q. Guo, K.Z. Gu, A.D. Shao, W.H. Zhu, Y.S. Xu, J. Wang, R. K. Prud'homme, X.H. Guo, Facile preparation of AIE-active fluorescent nanoparticles through flash nanoprecipitation, Ind. Eng. Chem. Res. 54 (2015) 4683–4688.
[6] D. Wang, J. Qian, F. Cai, S. He, S. Han, Y. Mu, 'Green' synthesized near-infrared PbS quantum dots with silica-PEG dual-layer coating: ultrastable and biocompatible optical probes for *in vivo* animal imaging, Nanotechnology 23 (2012) 245701.
[7] X. Ge, H. Zhao, T. Wang, J. Chen, J. Xu, G. Luo, Microfluidic technology for multiphase emulsions morphology adjustment and functional materials preparation, Chin. J. Chem. Eng. 24 (2016) 677–692.
[8] D. Wang, Z. Wang, Q. Zhan, Y. Pu, J.-X. Wang, N.R. Foster, L. Dai, Facile and scalable preparation of fluorescent carbon dots for multifunctional applications, Engineering 3 (2017) 402–408.
[9] Q. Zhan, X. Zhang, Y. Zhao, J. Liu, S. He, Tens of thousands-fold upconversion luminescence enhancement induced by a single gold nanorod, Laser Photon. Rev. 9 (2015) 479–487.
[10] D. Wang, L. Zhu, J.F. Chen, L. Dai, Liquid marbles based on magnetic upconversion nanoparticles as magnetically and optically responsive miniature reactors for photocatalysis and photodynamic therapy, Angew. Chem. Int. Ed. 55 (2016) 10795–10799.
[11] J.N. Leng, J.Y. Chen, D. Wang, J.X. Wang, Y. Pu, J.F. Chen, Scalable preparation of Gd_2O_3:Yb^{3+}/Er^{3+} upconversion nanophosphors in a high-gravity rotating packed bed reactor for transparent upconversion luminescent films, Ind. Eng. Chem. Res. 56 (2017) 7977–7983.
[12] L.-L. Li, R. Zhang, L. Yin, K. Zheng, W. Qin, P.R. Selvin, Y. Lu, Biomimetic surface engineering of lanthanide-doped upconversion nanoparticles as versatile bioprobes, Angew. Chem. Int. Ed. 51 (2012) 6121–6125.
[13] D. Ni, J. Zhang, W. Bu, H. Xing, F. Han, Q. Xiao, Z. Yao, F. Chen, Q. He, J. Liu, S. Zhang, W. Fan, L. Zhou, W. Peng, J. Shi, Dual-targeting upconversion nanoprobes across the blood brain barrier for magnetic resonance/fluorescence imaging of intracranial glioblastoma, ACS Nano 8 (2014) 1231–1242.
[14] J. Liu, R.T. Wu, N.N. Li, X. Zhang, Q. Zhan, S. He, Deep, high contrast microscopic cell imaging using three-photon luminescence of β-($NaYF_4$:Er^{3+}/$NaYF_4$) nanoprobe excited by 1480-nm CW laser of only 1.5-mW, Biomed. Opt. Expr. 6 (2015) 1857–1866.
[15] N.M. Idris, M.K. Gnanasammandhan, J. Zhang, P.C. Ho, R. Mahendran, Y. Zhang, In vivo photodynamic therapy using upconversion nanoparticles as remote-controlled nanotransducers, Nat. Med. 18 (2012) 1580–1585.
[16] Y.W. Zhang, L. Huang, Z.J. Li, G.L. Ma, Y.B. Zhou, G. Han, Illuminating cell signaling with near-infrared light-responsive nanomaterials, ACS Nano 10 (2016) 3881–3885.
[17] A. Bansal, H.C. Liu, M.K.G. Jayakumar, S. Andersson-Engels, Y. Zhang, Quasi-continuous wave near-infrared excitation of upconversion nanoparticles for optogenetic manipulation of C. elegans, Small 12 (2016) 1732–1743.
[18] W. Gao, H.R. Zheng, E.J. He, Y. Lu, F.Q. Gao, Luminescence investigation of Yb^{3+}/Er^{3+} co-doped single $LiYF_4$ microparticle, J. Lumin. 152 (2014) 44–48.
[19] H.S. Mader, M. Link, D.E. Achatz, K. Uhlmann, X. Li, O.S. Wolfbeis, Surface-modified upconverting microparticles and nanoparticles for use in click chemistries, Chem. Eur. J. 16 (2010) 5416–5424.
[20] Z. Li, K.H. Simith, G.W. Stevens, The use of environmentally sustainable bio-derived solvents in solvent extraction applications—a review, Chin. J. Chem. Eng. 24 (2016) 215–220.
[21] J.F. Jin, Y.J. Gu, C.W.Y. Man, J.P. Cheng, Z.H. Xu, Y. Zhang, H.S. Wang, V.H.Y. Lee, S.H. Cheng, W.T. Wong, Polymer-coated $NaYF_4$:Yb^{3+}, Er^{3+} upconversion nanoparticles for charge-dependent cellular imaging, ACS Nano 5 (2011) 7838–7847.
[22] H.X. Mai, Y.W. Zhang, R. Si, Z.G. Yan, L.D. Sun, L.P. You, C.Y. Yan, High-quality sodium rare-earth fluoride nanocrystals: controlled synthesis and optical properties, J. Am. Chem. Soc. 128 (2006) 6426–6436.
[23] F. Wang, Y. Han, C.S. Lim, Y. Lu, J. Wang, J. Xu, H. Chen, C. Zhang, M. Hong, X. Liu, Simultaneous phase and size control of upconversion nanocrystals through lanthanide doping, Nature 463 (2010) 1061–1065.
[24] A.D. Ostrowski, E.M. Chan, D.J. Gargas, E.M. Katz, G. Han, P.J. Schuck, D.J. Milliron, B.E. Cohen, Controlled synthesis and single-particle imaging of bright,

sub-10 nm lanthanide-doped upconverting nanocrystals, ACS Nano 6 (2012) 2686–2692.
[25] Y.W. Zhang, X. Sun, R. Si, L.P. You, C.H. Yan, Single-crystalline and monodisperse LaF_3 triangular nanoplates from a single-source precursor, J. Am. Chem. Soc. 127 (2005) 3260–3261.
[26] J.N. Shan, Y.G. Ju, Controlled synthesis of lanthanide-doped $NaYF_4$ upconversion nanocrystals via ligand induced crystal phase transition and silica coating, Appl. Phys. Lett. 91 (2007) 123103.
[27] S. Liang, Y. Liu, Y. Tang, Y. Xie, H.Z. Sun, H. Zhang, B. Yang, A User-friendly method for synthesizing high-quality $NaYF_4$:Yb, Er(Tm) nanocrystals in liquid paraffin, J. Nanomater. 2011 (2011) 302364.
[28] L. Yang, Y. Zhang, H. Li, H. Liu, Controllable synthesis of metallic Bi from commercial Bi_2O_3 via one-pot solvothermal reduction method, Chin. J. Chem. Eng. 25 (2017) 1202–1206.
[29] Z. Deng, L. Cao, F. Tang, B. Zou, A new route to zinc-blende CdSe nanocrystals: mechanism and synthesis, J. Phys. Chem. B 109 (2005) 16671–16675.
[30] D. Wang, L. Zhu, J.F. Chen, L. Dai, Can graphene quantum dots cause DNA damage in cells?, Nanoscale 7 (2015) 9894–9901
[31] J. Qian, D. Wang, F.H. Cai, W. Xi, L. Peng, Z.F. Zhu, H. He, M.-L. Hu, S. He, Observation of multiphoton-induced fluorescence from graphene oxide nanoparticles and applications in *in vivo* functional bioimaging, Angew. Chem. Int. Ed. 51 (2012) 10570–10575.
[32] D. Wang, J. Qian, W. Qin, A. Qin, B.Z. Tang, S. He, Biocompatible and photostable AIE dots with red emission for *in vivo* two-photon bioimaging, Sci. Rep. 4 (2014) 4279.
[33] P. Aggarwal, J.B. Hall, C.B. McLeland, M.A. Dobrovolskaia, S.E. McNeil, Nanoparticle interaction with plasma proteins as it relates to particle biodistribution, biocompatibility and therapeutic efficacy, Adv. Drug Deliv. Rev. 61 (2009) 428–437.
[34] T.A. Mary, K. Shanthi, K. Vimala, K. Soundarapandian, PEG functionalized selenium nanoparticles as a carrier of crocin to achieve anticancer synergism, RSC Adv. 6 (2016) 22936–22949.
[35] C. He, Y. Hu, L. Yin, C. Tang, C. Yin, Effects of particle size and surface charge on cellular uptake and biodistribution of polymeric nanoparticles, Biomaterials 31 (2010) 3657–3666.
[36] F. Alexis, E. Pridgen, L.K. Molnar, O.C. Farokhzad, Factors affecting the clearance and biodistribution of polymeric nanoparticles, Mol. Pharm. 5 (2008) 505–515.
[37] Y. Liu, K. Ai, J. Liu, Q. Yuan, Y. He, L. Lu, A high-performance ytterbium-based nanoparticulate contrast agent for *in vivo* X-ray computed tomography imaging, Angew. Chem. Int. Ed. 51 (2012) 1437–1442.
[38] D. Liu, W. Wu, J. Ling, S. Wen, N. Gu, X. Zhang, Effective PEGylation of iron oxide nanoparticles for high performance in vivo cancer imaging, Adv. Func. Mater. 21 (2011) 1498–1504.
[39] Q. Zhan, J. Qian, H. Liang, G. Somesfalean, D. Wang, S. He, Z. Zhang, S. Andersson-Engels, Using 915 nm laser excited Tm^3+/Er^3+/Ho^3+- doped $NaYbF_4$ upconversion nanoparticles for *in vitro* and deeper *in vivo* bioimaging without overheating irradiation, ACS Nano 5 (2011) 3744–3757.
[40] D. Wang, L. Zhu, Y. Pu, J.X. Wang, J.F. Chen, L. Dai, Transferrin-coated magnetic upconversion nanoparticles for efficient photodynamic therapy with near-infrared irradiation and luminescence bioimaging, Nanoscale 9 (2017) 11214–11221.
[41] Z. Xue, Z. Yi, X. Li, Y. Li, M. Jiang, H. Liu, S. Zeng, Upconversion optical/magnetic resonance imaging-guided small tumor detection and *in vivo* tri-modal bioimaging based on high-performance luminescent nanorods, Biomaterials 115 (2017) 90–103.